Nafta-Gaz 2026, vol. 82, no. 4, pp. 417–428, DOI: 10.18668/NG.2026.04.10

Finite-Element Investigation of Full-Scale PDC Bit–Rock Interaction in Impact-Scraping Composite Drilling: Effects of Rotational Speed and Weight on Bit

Badanie metodą elementów skończonych interakcji pełnowymiarowego świdra PDC ze skałą w złożonym wierceniu udarowo-skrawającym: wpływ prędkości obrotowej i nacisku na świder

Jialin Tian, Xin Li, Chenghang Liu

Oil and Gas Equipment Technology Sharing and Service Platform of Sichuan Province, School of Mechatronic Engineering, Southwest Petroleum University Chengdu, China

ABSTRACT: Conventional PDC drilling tools often exhibit low rock-breaking efficiency in hard formations. To address this limitation, an impact-scraping composite drilling tool was designed to generate coupled axial and torsional impacts through the coordinated action of a positive-displacement motor and a cam-roller mechanism. In this study, a full-scale PDC bit–rock finite-element model was established to compare the rock-breaking behavior of conventional drilling and impact-scraping drilling. The effects of the drilling parameters (rotational speed and weight on bit, WOB) on stress distribution, penetration response, axial acceleration, tangential cutting force, and specific rock-breaking energy were investigated. The results show that impact-scraping drilling enlarges the tensile-stress-dominated failure zone in the rock and improves the instantaneous penetration response. Under the baseline condition, the transient axial penetration velocity of the bit increased from 7.58 mm/s for conventional drilling to 16.63 mm/s for impact-scraping drilling, while the average tangential cutting force decreased from 5255.7 N to 3301.8 N. The tangential-force-based specific energy decreased by 38.5%, indicating a clear improvement in energy utilization. Increasing rotational speed and WOB can further increase the axial penetration velocity of the bit, but excessive values intensify bit vibration and may adversely affect cuttings removal. These results provide a numerical basis for parameter optimization and structural design of impact-assisted PDC drilling tools for hard formations.

Keywords: axial torsional composite-impact drilling, impact-scraping drilling tool, PDC bit, rock-breaking efficiency, finite-element simulation, specific energy.

STRESZCZENIE: Konwencjonalne narzędzia wiertnicze PDC często cechują się niską skutecznością urabiania skały w twardych formacjach. W celu wyeliminowania tego ograniczenia zaprojektowano narzędzie do złożonego wiercenia udarowo-skrawającego, które dzięki skoordynowanemu działaniu silnika wyporowego i mechanizmu krzywkowo-rolkowego generuje sprzężone udary osiowe i skrętne. W ramach badania opracowano pełnowymiarowy model elementów skończonych układu świder PDC–skała, umożliwiający porównanie przebiegu urabiania skały podczas wiercenia konwencjonalnego i udarowo-skrawającego. Przeanalizowano wpływ parametrów wiercenia, w tym prędkości obrotowej oraz nacisku na świder (WOB), na rozkład naprężeń, przebieg penetracji, przyspieszenie osiowe, styczną siłę skrawania i jednostkową energię urabiania skały. Wyniki wykazały, że wiercenie udarowo-skrawające powoduje zwiększenie w skale strefy zniszczenia, w której dominują naprężenia rozciągające, oraz poprawia chwilową zdolność penetracji. W warunkach bazowych chwilowa osiowa prędkość penetracji świdra wzrosła z 7,58 mm/s w przypadku wiercenia konwencjonalnego do 16,63 mm/s w przypadku wiercenia udarowo-skrawającego, natomiast średnia styczna siła skrawania zmniejszyła się z 5255,7 N do 3301,8 N. Jednostkowa energia obliczona na podstawie siły stycznej zmniejszyła się o 38,5%, co świadczy o wyraźnej poprawie efektywności wykorzystania energii. Zwiększenie prędkości obrotowej i nacisku na świder może dodatkowo zwiększyć osiową prędkość penetracji, jednak zbyt wysokie wartości tych parametrów nasilają drgania świdra i mogą niekorzystnie wpływać na odprowadzanie zwiercin. Uzyskane wyniki stanowią numeryczną podstawę do optymalizacji parametrów oraz projektowania konstrukcji narzędzi wiertniczych PDC ze wspomaganiem udarowym przeznaczonych do wiercenia w twardych formacjach.

Słowa kluczowe: złożone wiercenie z udarem osiowo-skrętnym, narzędzie do wiercenia udarowo-skrawającego, świder PDC, efektywność urabiania skały, symulacja metodą elementów skończonych, energia jednostkowa.

Corresponding author: Xin Li, e-mail: *17623162768@163.com*

Article contributed to the Editor: 22.05.2026. Approved for publication: 26.08.2026.

Introduction

When PDC bit is drilled in hard formation, the rate of penetration is low and the bit stick-slip vibration failure is fast (Dolezal et al., 2011). To solve this problem, some researchers have developed a more efficient multidimensional composite impact rock breaking technology based on one-dimensional impact assisted rock breaking technology. This technology integrates two single directional impact drilling technologies, axial impact and torsional impact, and combines the advantages of these two technologies (Mu et al., 2018). Therefore, it is the main research direction of impact rock breaking at present.

In 2008, Shell Company of the United States proposed a kind of impact drill bit, which can generate axial impact on rock while rotating around the axis to cut rock, effectively improving the drilling efficiency. Later, a hybrid bit was proposed that greatly improved ROP and became an alternative to the conventional bit with faster and more durable bit performance (Huang et al., 2020, Kong et al., 2022). Deng et al. (2022) designed a compound impact tool that indirectly controls axial impact by torsion by controlling stroke through an internal flow distribution mechanism. Huang et al. (2023) and Lu et al. (2023) established a coupled axial and torsional vibration model. Based on this, Yang et al. (2024) analyzed the impact performance and influencing factors of composite impact drilling tool through large eddy simulation method. Song et al. (2021) proposed the axial torsional composite impact rock breaking technology, and analyzed the capability transfer efficiency of the composite rock breaking tool on the basis of establishing the nonlinear dynamic model. Zeng et al. (2020), Liu et al. (2021) studied the fracture mechanism of rock by simulating rock breaking with compound impact drilling tools, and compared damage evolution of rock and formation process of rock debris under three different working conditions: axial impact, torsional impact and axial torsional composite impact. The results show that rock breaking effect of axial torsional composite impact drilling is the best. Zha et al. (2017) and Koronatov et al. (2023) established the vibration model of PDC bit under axial impact and axial torsional composite impact, simulated shear force of rock under the two states, and analyzed motion rule of PDC bit. The results show that PDC bit composite impact rock breaking technology can increase the cutting depth of bit cutter and restrain torsional vibration of bit, so as to improve the ROP. Li et al. (2021) analyzed the effects of impact velocity, dynamic load amplitude, ratio of axial force and torsional force of drilling tool on cutting force and cutting depth. It is pointed out that both cutting force and cutting depth increase with increasing ratio ($\mu < 2$) When $\mu = 1.5$, penetration depth and rate are obtained regardless of rock type. Under the composite impact, penetration depth and penetration rate increased by 49.02% and 35.92%, respectively. Based on study on mechanism of rock breakage, Peng et al. (2021) found that in the process of rock breakage, rock is in state of coexistence of tensile stress and compressive stress. It is concluded that the cause of rock failure is comprehensive effect of "stretching and shearing", and influence of bit impact frequency, WOB and rotational speed on rock failure is further analyzed. Xi et al. (2023) studied the effect of bit geometry on dynamic load parameters, and the research results showed that adding axial impact, torsional impact or axial torsional composite impact could increase the drill penetration depth by 31.3%, 5.6% and 34.7%, respectively. Sun et al. (2024) compared and analyzed rock breaking effect under static load, axial impact load, torsional impact load and axial torsional composite impact load. Furthermore, the effects of temperature (Sun et al., 2024, Ji et al., 2024), impact frequency and amplitude, WOB, lithology (Mu et al., 2022), rotational speed and impact Angle (Liu et al., 2022) on rock breaking effect are further analyzed. Under the best working conditions, composite impact can increase drill depth and mechanical penetration rate by nearly 2 times.

In summary, the research on existing achievements shows that composite impact drilling technology has significant advantages in improving drilling efficiency, but most of the research is about the qualitative analysis of rock breaking mechanism. In particular, there are few studies on impact of complex impact frequency and related parameters on rock breaking effect of drill bits, and even if there are studies, most of them stay in the single tooth impact rock breaking, and few involve rock breaking analysis of full-size drill bits. In this paper, a full-size PDC bit model is established, and the advantages of composite impact drilling over conventional drilling are analyzed based on rock breaking mechanism. The influence of different speed and WOB on the rock breaking effect of the composite drill tool is simulated and analyzed. The research results have important reference significance for the study of composite impact rock breaking.

Materials and Methods

Structure of the impact-scraping composite drilling tool

As shown in Figure 1, the impact-scraping drilling tool consists of an energy-supply system and a driveline-impact system. During rock breaking, the bottom-hole rock is subjected to the combined effects of WOB, impact load, and torque. On this basis, a simplified nonlinear dynamic finite element model of bit-rock interaction was established, as shown in Figure 2, and numerical simulations of the rock-breaking process were conducted. In the present study, fluid flow and fluid–solid

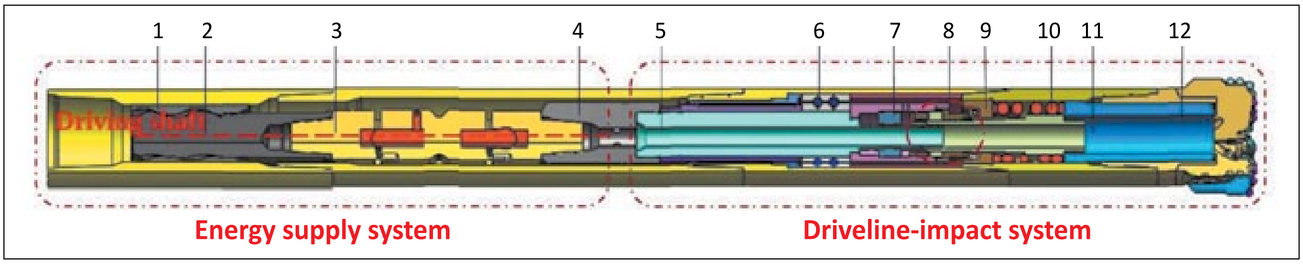

Figure 1. Structure diagram of impact-scraping drilling tool. 1. Rubber bushing; 2. Rotor; 3. Universal joint; 4. Water cap; 5. Driving shaft; 6. Bearing; 7. Piston; 8. Cam-roller system; 9. Spring base; 10. Spring; 11. Jarring axis; 12. Impact bit

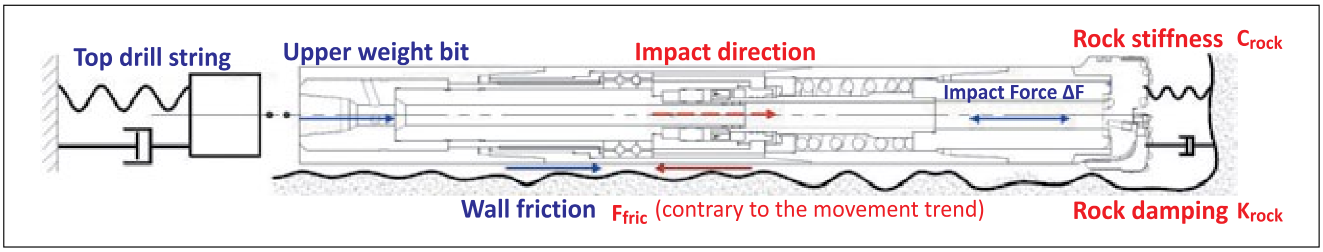

Figure 2. Rock breaking theoretical model of impact-scraping drilling tool

coupling were not explicitly considered because the analysis focused on the mechanical rock-breaking response induced by WOB, rotation, and impact loading.

Modelling assumptions

The bottom-hole environment is highly complex under actual drilling conditions. To improve computational efficiency while retaining the dominant rock-breaking mechanisms, several secondary factors were simplified in the numerical model. The following assumptions were adopted:

1. the strength and hardness of the bit are much higher than those of the rock; therefore, the bit is treated as a rigid body and bit deformation is neglected;
2. failed rock elements are assumed to be removed immediately from the model, and the influence of detached debris on subsequent bit-rock contact is ignored; and
3. the effects of drilling-fluid flow and thermal-mechanical coupling are not considered in the present model.

Mathematical formulation of bit-rock contact

The rock-breaking process of the impact-scraping drilling tool is a typical nonlinear dynamic contact problem. Its nonlinearity mainly arises from three aspects:

1. geometric nonlinearity caused by large displacement and rotation within a short time;
2. material nonlinearity caused by large rock strain before failure; and
3. contact nonlinearity caused by the continuously changing contact state between the cutter surface and the rock.

The contact system is formulated using the finite element method. The spatial domain occupied at time t is denoted by Ω. The body force, boundary force, and Cauchy internal stress acting on the contact system are denoted by b, t, and σ, respectively. The contact problem can therefore be expressed as follows:

$$\int_{\Omega}\sigma\delta e d\Omega - \int_{\Omega} b\delta u d\Omega - \int_{\Gamma_f} q\delta e dS - \int_{\Gamma_c} q_c \delta u dS + \\ + \int_{\Omega}\rho a \delta u d\Omega = 0 \tag{1}$$

where: Γ_f is the boundary of boundary force; Γ_c is the contact boundary; δu is virtual displacement; δe is virtual strain; ρ is density; a is the acceleration.

The finite element model is used to discretize the domain Ω to obtain the virtual displacement, so that:

$$\boldsymbol{m}\ddot{\boldsymbol{u}} = \boldsymbol{p}(t) + \boldsymbol{c}(u,\alpha) - \boldsymbol{f}(u,\beta) \tag{2}$$

where:

$\boldsymbol{m}$ is the mass matrix,

$\ddot{\boldsymbol{u}}$ is the acceleration vector,

$\boldsymbol{p}(t)$ is the time-dependent external-load vector,

$\boldsymbol{c}(u,\alpha)$ is the contact and friction-force vector,

$\boldsymbol{f}(u,\beta)$ is the internal-force vector,

$\boldsymbol{u}$ is the displacement vector, α represents contact-related parameters, and

$\boldsymbol{\beta}$ represents material constitutive parameters.

Rock constitutive model and failure criterion

According to Lemaitre's strain equivalence hypothesis (Lemaitre, 1985), the rock damage constitutive model is expressed as follows:

$$\text{penetration rate } S_{\sigma}^{*} = \frac{S_{\sigma}}{1-D} = \frac{CS_{\varepsilon}}{1-D} \tag{3}$$

where,
S_σ^* – is the effective stress matrix,
S_σ – is the nominal stress matrix,
D – is rock damage variable,
S_ε – is the strain matrix,
C – is the elastic matrix of rock.

The failure of rock elements is assumed to be stochastic, and the element strength follows a Weibull distribution (Cao et al., 2004). The probability density function of rock strength is expressed as follows:

$$p(F)=\frac{m}{F_0}\left(\frac{F}{F_0}\right)^{m-1}\exp\left[-\left(\frac{F}{F_0}\right)^m\right] \tag{4}$$

where: F is a randomly distributed variable with Weibull distribution of unit strength; m is a parameter reflecting rock brittleness; F_0 is the macroscopic strength of the rock.

The proportion of the damaged part in the whole rock is defined as the rock damage variable D, and it is expressed as:

$$D=\int_0^F p(x)dx=1-\exp\left[-\left(\frac{F}{F_0}\right)^m\right] \tag{5}$$

If rock always satisfies Hooke's law before failure, for triaxial compression experiments with equal confining pressure, Equations (3) and (5) can be obtained as follows.

$$\sigma_1=E\varepsilon_1(1-D)+2\mu\sigma_3=E\varepsilon_1\exp\left[-\left(\frac{F}{F_0}\right)^m\right]+2\mu\sigma_3 \tag{6}$$

where: σ_1^* is the axial effective stress; σ_3^* is the lateral effective stress; σ_1 is the nominal axial stress; σ_3 is the nominal lateral stress; μ is Poisson's ratio; ε_1 is the axial strain; E is the elastic modulus.

The yield point of the rock stress-strain curve is approximated as the damage threshold. When the strain is lower than the threshold strain, the initial damage variable is set to zero (Teale, 1965), and the relationship between yield stress and plastic strain is expressed as follows:

$$\sigma_1=\sigma_{1y}\frac{\varepsilon_1}{\varepsilon_{1y}} \tag{7}$$

where: σ_{1y} is the stress threshold corresponding to the strain threshold ε_{1y}.

When the strain is equal to or greater than the strain threshold ε_{1y}, the corresponding rock constitutive equation is shown in Equation (6). The Drucker-Prager failure criterion based on principal stress representation is expressed as follows:

$$F=f(\sigma^*)=\alpha_0 I_1+\sqrt{J_2} \tag{8}$$

Among,

$$\alpha_0=\frac{\sin\varphi}{\sqrt{9+3\sin^2\varphi}} \tag{9}$$

$$I_1=\sigma_1^*+\sigma_2^*+\sigma_3^*=\frac{(\sigma_1+2\sigma_3)E\varepsilon_1}{\sigma_1-2\mu\sigma_3} \tag{10}$$

$$\sqrt{J_2}=\sqrt{\frac{1}{6}\left[\left(\sigma_1^*-\sigma_2^*\right)^2+\left(\sigma_2^*-\sigma_3^*\right)^2+\left(\sigma_3^*-\sigma_1^*\right)^2\right]}=$$
$$=\frac{(\sigma_1-\sigma_3)E\varepsilon_1}{\sqrt{3}(\sigma_1-2\mu\sigma_3)} \tag{11}$$

The peak stress and peak strain of the rock stress-strain curve are respectively set to σ_{1p} and ε_{1p}, and Equation (6) can be rewritten as follows.

$$\sigma_{1p}=E\varepsilon_{1p}(1-D_p)+2\mu\sigma_3=E\varepsilon_{1p}\exp\left[-\left(\frac{F_p}{F_0}\right)^m\right]+2\mu\sigma_3 \tag{12}$$

where: D_p is the rock damage variable at the peak point; F_p is the unit strength at the peak point.

In Equation (6), the partial differential of stress σ_1 to strain ε_1 is obtained, and $\partial\sigma_1/\partial\varepsilon_1\Big|_{\varepsilon_1=\varepsilon_{1p}}=0$ is considered.

$$\left(\frac{F_p}{F_0}\right)=-\ln\frac{\sigma_{1p}-2\mu\sigma_3}{E\varepsilon_{1p}} \tag{13}$$

In summary, the basic equations of complete rock damage constitutive model based on D-P failure criterion and Weibull distribution are obtained.

1. When the strain of rock is less than strain threshold ε_{1y}, the constitutive equation of rock is:

$$\sigma_1=\sigma_{1y}\frac{\varepsilon_1}{\varepsilon_{1y}} \tag{14}$$

2. When the strain is equal to or greater than the strain threshold ε_{1y}, the corresponding rock constitutive equation is:

$$\sigma_1=E\varepsilon_1\exp\left[-\left(\frac{F}{F_0}\right)^m\right]+2\mu\sigma_3 \tag{15}$$

3. The expression of brittleness parameter m is:

$$m=$$
$$=\frac{-F_p}{E\varepsilon_{1p}\dfrac{\alpha_0\left(\sigma_{1p}+2\sigma_3\right)+\sqrt{3}\left(\sigma_{1p}-\sigma_3\right)/3}{\sigma_{1p}-2\mu\sigma_3}\ln\dfrac{\sigma_{1p}-2\mu\sigma_3}{E\varepsilon_{1p}}} \tag{16}$$

4. The expression of the intensity parameter F_0 is:

$$F_0=\left(F_p^m\Big/-\ln\frac{\sigma_{1p}-2\mu\sigma_3}{E\sigma_{1p}}\right)^{\frac{1}{m}} \tag{17}$$

Finite element model, material properties, and boundary conditions

In the simulation, the radius of the rock model was set to 200 mm to reduce the influence of remote boundary conditions on the internal stress field. The bit model was coupled to a reference point and contacted the rock surface through a defined contact surface. When upper rock elements failed, the bit re-contacted the newly generated cutting surface. The bottom of the rock model was fixed. Considering the influence of confining pressure and neglecting pore pressure, the overburden pressure and horizontal in-situ stresses were applied according to the following relationships:

$$P_u = G_u * h \tag{18}$$

$$P_c = G_c * h \tag{19}$$

where: h is Borehole depth, m; G_u is overburden pressure gradient, MPa/m; G_c is horizontal ground stress gradient, MPa/m.

The specific data are shown in Table 1.

Table 1. Setting of rock boundary conditions

Overburden pressure P_u [MPa]	Horizontal ground stress P_c [MPa]
46	32

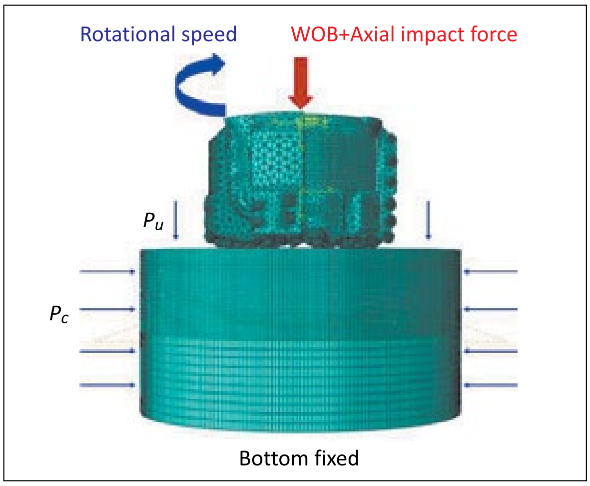

Figure 3. Finite element analysis model

The bit was constrained to a reference point. The bit was meshed using tetrahedral elements, whereas the rock model was meshed using C3D8R hexahedral elements with hourglass control. Mesh refinement was applied in the bit-rock contact region. Surface-to-surface contact was used between the bit and the rock, and the element-deletion method was adopted to remove failed rock elements during numerical simulation. The rock material parameters used in the simulation are listed in Table 2.

Figure 3 shows the load setting for the rock-breaking simulation of the impact-scraping drilling tool. Axial impact forces with frequencies of 6.0, 7.5, and 9.0 Hz were applied to the bit under the corresponding working conditions.

Mesh-independence and model verification

To verify mesh independence, models with total element numbers of 6.2×10^5, 8.2×10^5, 1.04×10^6, and 1.23×10^6 were compared using the maximum equivalent stress as the evaluation index. The results are shown in Figure 4.

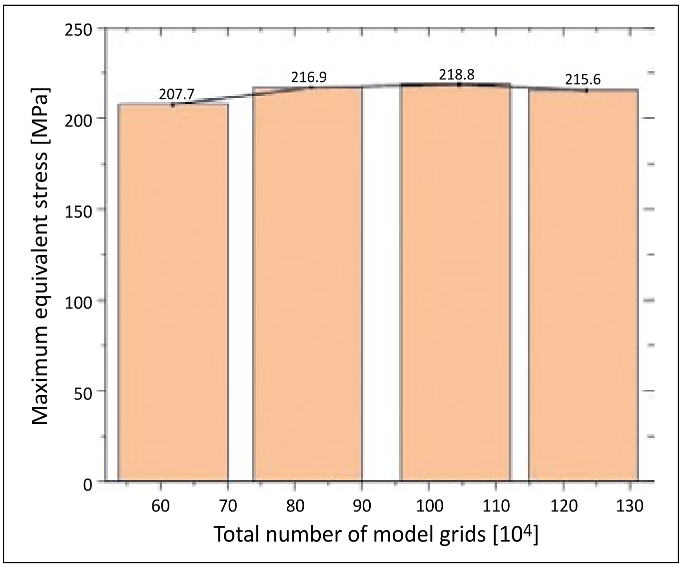

Figure 4. Comparison of equivalent stress with different mesh numbers

In engineering simulations, if the stress deviation before and after mesh refinement is controlled within 3% and the computational cost remains acceptable, the mesh effect can be regarded as negligible. As shown in Figure 4, when the total number of elements increases from 8.2×10^5 to 1.23×10^6, the variation in maximum equivalent stress remains within 3%. Therefore, a model with approximately 8.3×10^5 elements was adopted for the subsequent simulations.

In addition to the mesh-independence analysis, the reliability of the numerical model was assessed by comparison

Table 2. Material parameters of the model

Materials	Density [kg/m^3]	Poisson's ratio	Elasticity modulus [GPa]	Shear Angle [°]	Flow stress ratio	Internal friction angle(deg)
limestone	2460	0.178	31.2	25	0.8	27.61

with published numerical and experimental studies. Dong and Chen (2018) established a full-scale PDC-bit model for percussive-rotary drilling and verified the numerical approach using an actual drilling case. Xi et al. (2022) combined numerical simulations with single-cutter experiments and demonstrated that rotary-percussion loading promoted cutter penetration and rock damage. Zhang et al. (2023) further reported, through numerical simulations and laboratory micro-PDC drilling tests, that vibration-assisted drilling enhanced the penetration response and reduced the drilling resistance within an appropriate parameter range. Similar numerical–experimental approaches have also been employed for full-scale PDC-bit performance analysis.

The present results exhibit qualitatively consistent trends. Compared with conventional drilling, impact-scraping drilling produces a stronger dynamic damage response, promotes tensile-stress-assisted failure, increases the simulated penetration response, and reduces the tangential cutting-force component. This qualitative agreement supports the capability of the present model to compare different drilling modes and operating parameters under identical numerical conditions.

Simulation results and analysis

Rock stress analysis

Finite element simulations were conducted for different drilling methods. The corresponding load settings are listed in Table 3.

Table 3. Load parameter settings

Drilling mode	WOB [kN]	Rotational speed [rpm]	Axial impact load [N]	Impact frequency [Hz]
Conventional drilling	10	120	0	0
Impact-scraping drilling	10	120	14135.4	6.0

The compressive strength of rock is much higher than its tensile strength. Therefore, the maximum principal stress distribution of the rock elements was used to evaluate the rock-failure tendency, as shown in Figure 5. During conventional drilling (Figure 5a), tensile and compressive stresses coexist in the rock, but compressive stress is mainly concentrated near the bit-rock contact region. During impact-scraping drilling (Figure 5b), the tensile-stress region in the rock element contacted by the cutter is significantly enlarged compared with that under conventional drilling. Stress is transmitted in the form of waves, part of which is repeatedly reflected between the cutter and the rock, thereby promoting tensile failure and crack propagation. This indicates that impact-scraping drilling can create more favorable stress conditions for brittle rock failure.

Drilling rate analysis

In the present finite-element model, the axial displacement of the bit is used to characterize its penetration response. The bit transient axial penetration velocity (mm/s) was determined from the slope of the axial displacement–time curve. This parameter represents the axial penetration response of the bit during the simulated interval and is used only for comparison between different drilling modes under identical numerical conditions. The comparison is shown in Figure 6.

The results show the following characteristics. First, the bit-rock contact state varies continuously during drilling. Before the bit contacts the rock, the axial displacement increases relatively rapidly. After contact is established, rock resistance reduces the penetration speed, and collision between the bit and rock causes slight rebound; therefore, the axial displacement curve fluctuates. Second, the bit transient axial penetration velocity of conventional drilling is 7.58 mm/s, whereas that of impact-scraping drilling reaches 16.63 mm/s, approximately

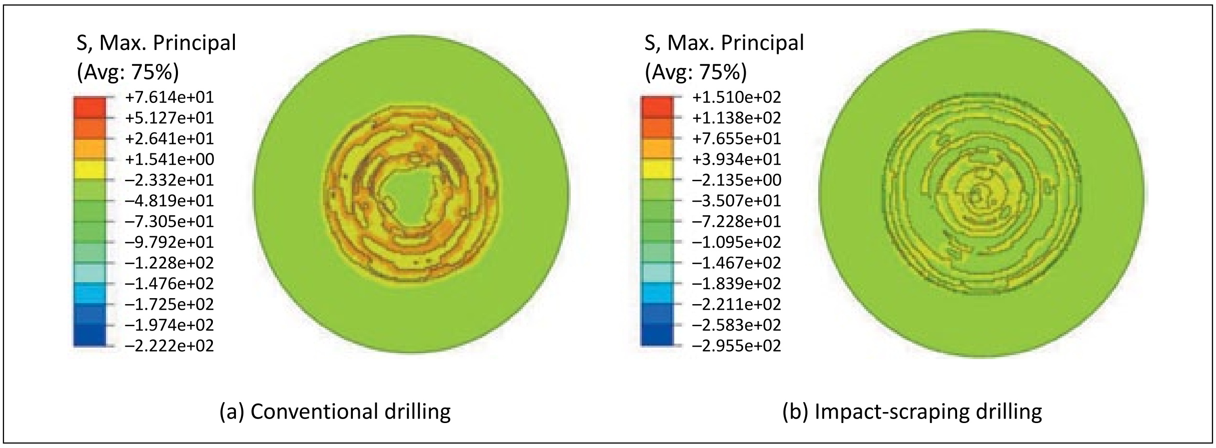

Figure 5. Cloud map of maximum principal stress of rock

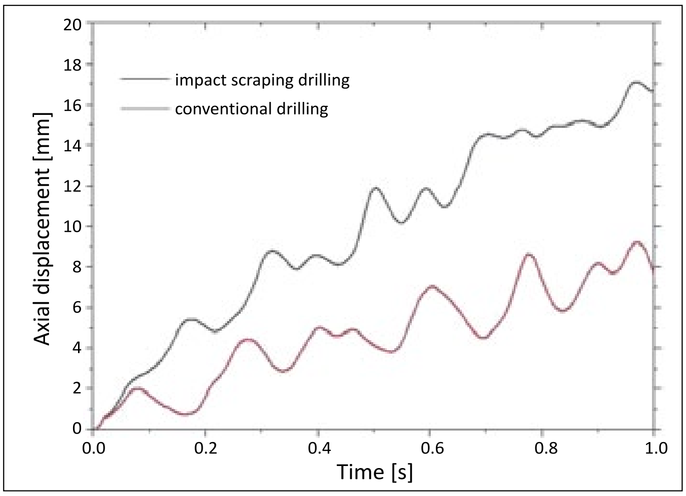

Figure 6. Axial displacement–time curves of the bit under different drilling modes

2.2 times that of conventional drilling. This improvement occurs because the axial impact force acts directly on the rock surface through the impact teeth, forming local impact craters, and also propagates into the rock in the form of stress waves. These effects promote crack initiation and propagation, thereby improving the penetration response of the impact-scraping drilling tool.

Analysis of axial acceleration

The impact stress wave caused by axial bit vibration acts on the bottom-hole rock, while the rock simultaneously exerts a reaction force on the bit. Excessive axial vibration may be harmful to PDC cutters, whose dominant rock-breaking mode is shear cutting; it can reduce bit service life and may even cause cutter breakage, drill-string damage, or downhole accidents. Therefore, axial acceleration was used to characterize bit vibration. Figure 7 compares the axial acceleration curves of conventional drilling and impact-scraping drilling.

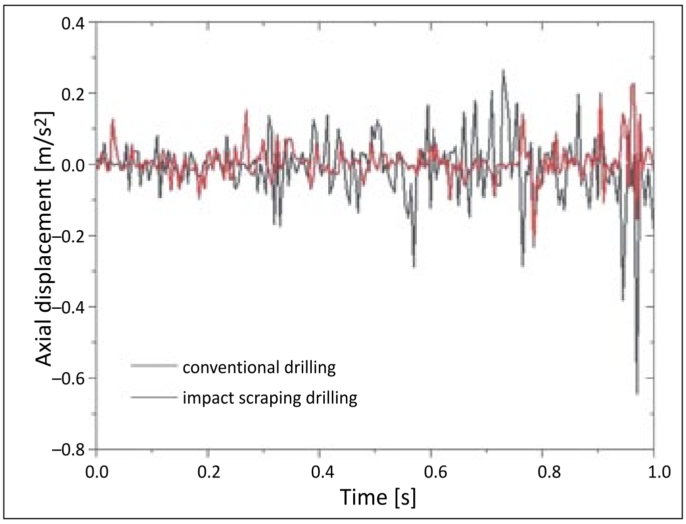

Figure 7. Comparison of axial acceleration curves

The two curves indicate that the axial accelerations of both drilling methods exhibit obvious aperiodic fluctuations. This aperiodicity results from the time-varying bit-rock interaction. The fluctuations are caused by intermittent loss and re-establishment of bit-rock contact after local rock elements fail. When the bit loses contact restraint after a rock element is removed, the axial acceleration increases instantaneously. As the bit establishes new face-to-face contact with the rock, the acceleration decreases and may even become negative. At the initial stage, the vibration is relatively weak. As the bit penetrates deeper into the rock and the contact area increases, the vibration becomes more pronounced. Compared with conventional drilling, impact-scraping drilling shows a more controlled axial acceleration response under the baseline condition, indicating that the composite impact mode improves rock breaking without causing excessive bit vibration.

Analysis of tangential-force-based specific energy

When a bit cutter breaks rock, the fluctuation of tangential force reflects the fracture and removal of rock elements. The tangential force of the cutter under the two drilling methods was extracted through post-processing, and the comparison curve is shown in Figure. 8.

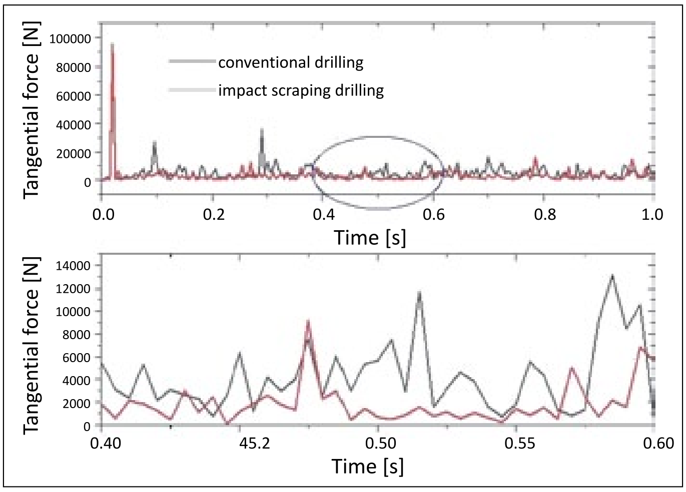

Figure 8. Tangential force curve of cutter under two drilling methods

When the cutter first contacts the rock element, the tangential force changes sharply and then gradually fluctuates around a stable level as the cutting process enters a steady state. The average cutting force during impact-scraping drilling is 3301.8 N, which is 37.2% lower than the 5255.7 N obtained during conventional drilling.

The specific rock-breaking energy can quantitatively reflect the rock-breaking efficiency of different drilling methods from the perspective of energy consumption. It is defined as follows (Teale, 1965):

$$MSE = W/V \quad (20)$$

where: MSE is the specific rock-breaking energy; W is the work consumed during rock breaking; and V is the volume of broken rock.

Using the projected crushing volume to calculate the specific rock-breaking energy, Equation 20 can be transformed into:

$$MSE = \frac{W}{V} = \frac{f_h d}{Sd} = \frac{f_h}{S} \quad (21)$$

where: f_h is local tangential force; d is the rock breaking depth of bit; S is cutting projection area.

The interaction model between PDC single tooth and rock is shown in Figure 9. The projected cutting area can be calculated by the following Equation:

$$S = \begin{bmatrix} r^2 \cos^{-1}\left(1 - \frac{d/\cos\theta}{r}\right) - \\ -r\left(r - \frac{d}{\cos\theta}\right)\sin\left(\cos^{-1}\left(1 - \frac{d/\cos\theta}{r}\right)\right) \end{bmatrix} \cos\beta \quad (22)$$

where: r is radius of bit cutter; θ is Caster Angle; β is Camber Angle.

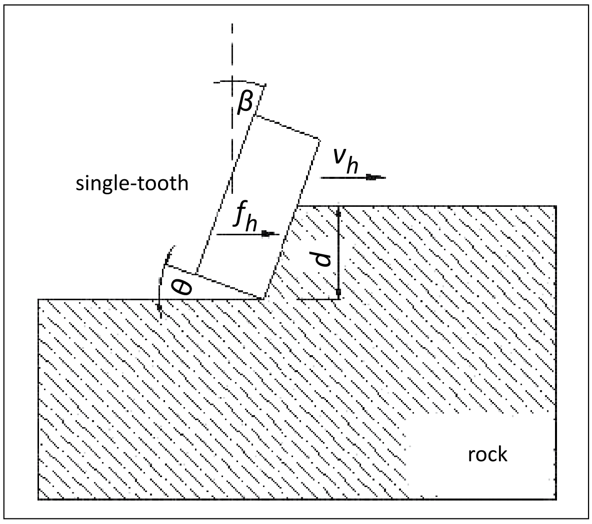

Figure 9. Interaction model between PDC single tooth and rock

As shown in Figure 10, the tangential-force-based specific energy was 86.28 mJ/mm^3 for conventional drilling and 53.07 mJ/mm^3 for impact-scraping drilling, corresponding to a reduction of approximately 38.5%. This result indicates that the tangential cutting-energy requirement of the PDC cutters was reduced after the rock had been pre-damaged by the impact action, and demonstrates that impact-scraping drilling is more conducive to rock failure and improves rock-breaking efficiency. It should be noted that the present specific-energy calculation includes only the tangential cutting-force contribution. The axial work associated with WOB and the additional work introduced by the impact load were not included.

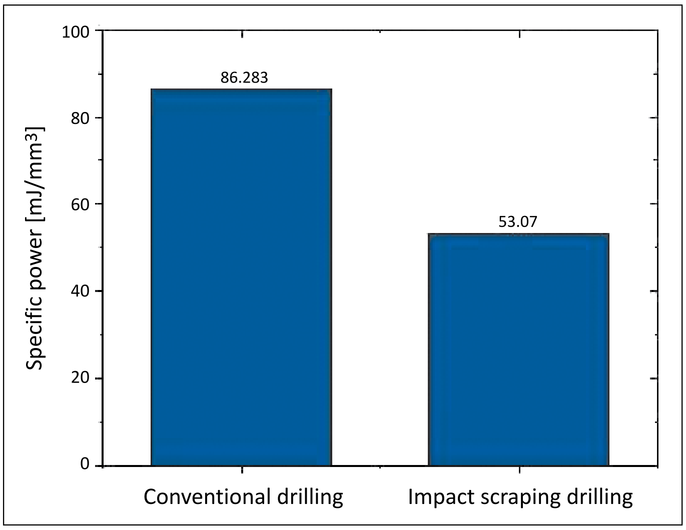

Figure 10. Rock breaking specific work under different drilling methods

Analysis of influence of rotational speed on rock breaking

Rotational speed, impact load, and impact frequency interact with each other and strongly influence the rock-breaking effect of the impact-scraping drilling tool. Simulations were conducted at rotational speeds of 120, 150, and 180 rpm. The corresponding parameters are listed in Table 4.

Table 4. Load parameter settings

Working condition	WOB [kN]	Rotational speed [rpm]	Axial impact load [N]	Impact frequency [Hz]
1	10	120	14135.4	6.0
2	10	150	14411.3	7.5
3	10	180	13189.9	9.0

The main failure modes of bottom-hole rock are shear failure and tensile failure. Because the shear stress in the model is relatively small compared with the compressive and tensile stresses, the maximum principal stress was mainly used for comparison. As shown in Figures 11–13, the maximum principal stress distribution varies with rotational speed.

At 120 rpm, the rock experiences more compressive stress regions. As the rotational speed increases, the stress state gradually changes from compression-dominated to tension-dominated, and the tensile-stress region expands. This stress transition is favorable for rock fracture and removal.

The penetration curves of the impact-scraping drilling tool at the three rotational speeds (Figure 14) show continuous fluctuating increases, which is consistent with bit rebound during

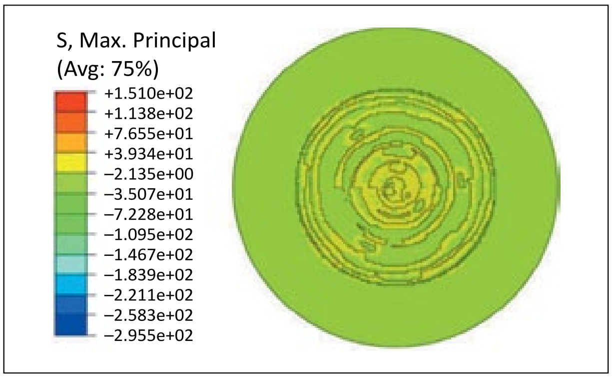

Figure 11. Maximum principal stress nephogram of rock at 120 rpm

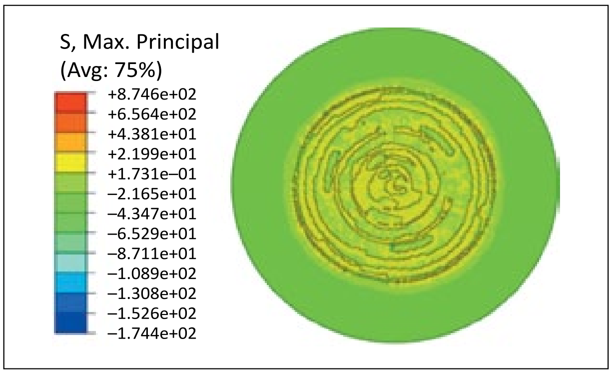

Figure 12. Maximum principal stress nephogram of rock at 150 rpm

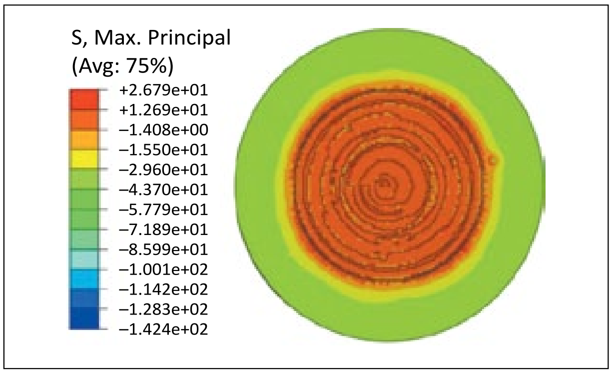

Figure 13. Maximum principal stress nephogram of rock at 180 rpm

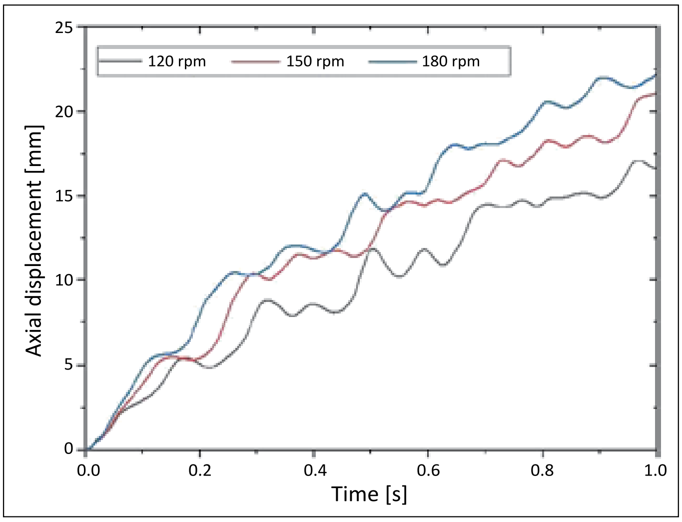

Figure 14. Axial displacement at different rotational speeds

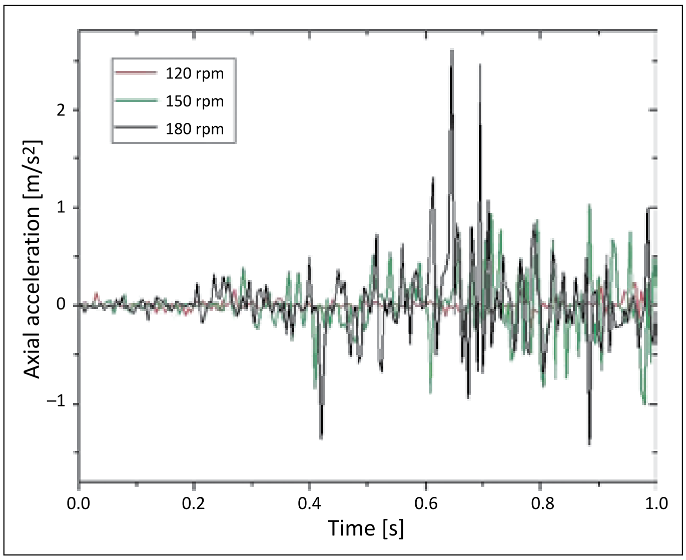

Figure 15. Axial acceleration at different rotational speeds

actual drilling. As the rotational speed increases from 120 to 180 rpm, the bit transient axial penetration velocity gradually increases. The bit transient axial penetration velocity values at 120, 150, and 180 rpm are 16.63, 21.06, and 22.20 mm/s, respectively. These results indicate that increasing rotational speed can significantly improve bit transient axial penetration velocity at low-to-moderate speeds. However, once the rotational speed exceeds a certain level, its marginal contribution to bit transient axial penetration velocity decreases, and further speed increase becomes less effective.

The axial acceleration of the bit under different rotational speeds was extracted for analysis, as shown in Figure 15.

The fluctuation amplitude of axial acceleration increases with rotational speed, and both the amplitude and frequency of vibration become higher. In the initial contact stage (0–0.4 s), the acceleration responses under the three rotational speeds are similar. As time increases, the influence of rotational speed becomes more evident. The acceleration ranges at 120, 150, and 180 rpm are –0.23 to 0.22 m/s^2, –1.00 to 1.03 m/s^2, and –1.42 to 2.61 m/s^2, respectively. Therefore, bit vibration becomes more severe at high rotational speed. Considering both bit transient axial penetration velocity and vibration intensity, 150 rpm is considered more suitable for the impact-scraping drilling tool under the simulated conditions.

Analysis of influence of WOB on rock breaking

WOB is another major factor affecting rock-breaking efficiency. During drilling, WOB presses the bit against the rock surface and reduces energy loss during cutter-rock impact. Under impact loading, WOB can increase the peak contact force and help cutters maintain sufficient force for rock fracture.

Table 5. Load parameter settings

Working condition	WOB [kN]	Rotational speed [rpm]	Axial impact load [N]	Impact frequency [Hz]
1	10	120	14135.4	6.0
2	40	120	14135.4	6.0
3	80	120	14135.4	6.0

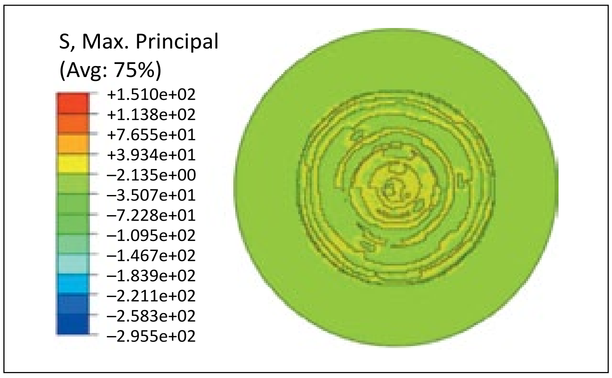

Figure 16. Maximum principal stress nephogram of rock with WOB of 10 kN

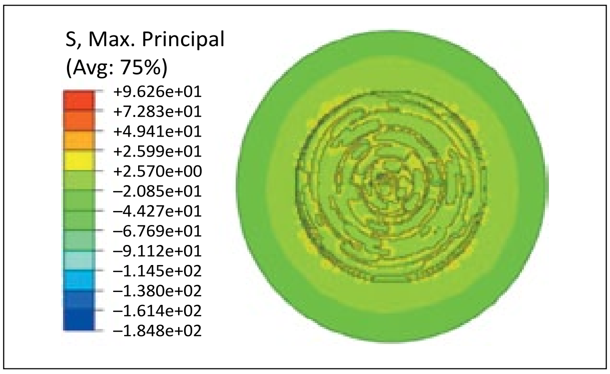

Figure 17. Maximum principal stress nephogram of rock with WOB of 40 kN

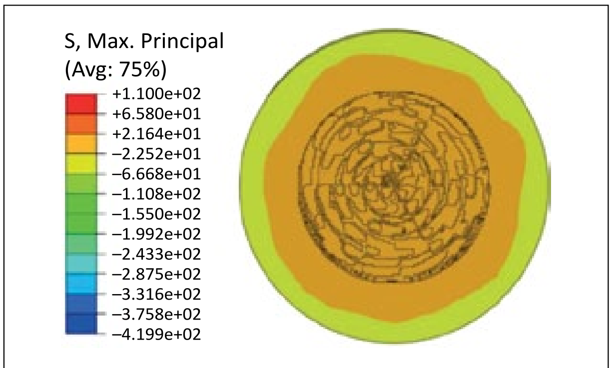

Figure 18. Maximum principal stress nephogram of rock with WOB of 80 kN

The principal stress distributions of the rock under different WOB values are shown in Figures 16–18. When the drilling tool operates, rock failure is mainly associated with tensile stress. As WOB increases, the compressive-stress region in the rock gradually expands, which may be unfavorable for efficient tensile failure.

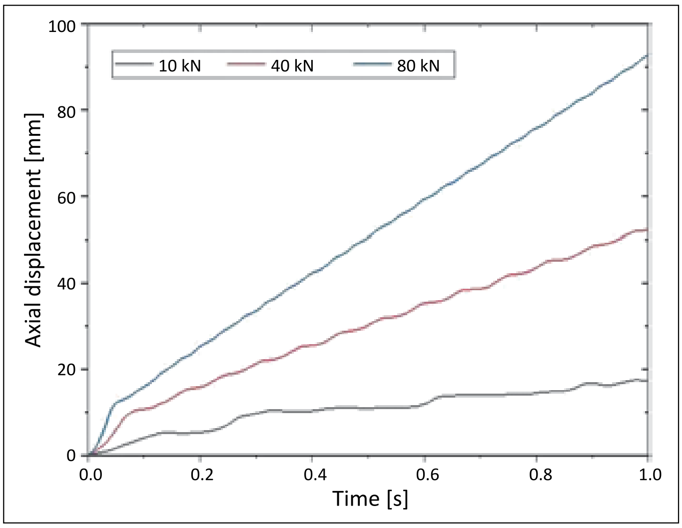

Figure 19. Variation of axial displacement with different WOB over time

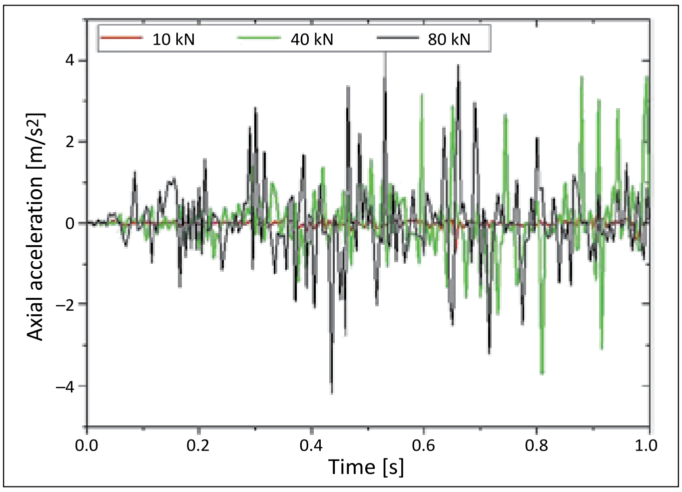

Figure 20. Variation of axial acceleration with different WOB over time

The penetration curves of the impact-scraping drilling tool under different WOB values show obvious fluctuations and continuous increases. Before contact, the bit displacement increases almost linearly until the bit reaches the rock surface. After contact, the bit cuts and fractures rock elements under the combined action of WOB, rotation, and impact loading. As WOB increases from 10 to 80 kN, the axial displacement increases significantly. The bit transient axial penetration velocity values at 10, 40, and 80 kN are 16.63, 52.27, and 92.86 mm/s, respectively. These results indicate that increasing WOB can markedly improve bit transient axial penetration velocity. However, excessive WOB may compact the rock cuttings at the bottom hole, making them difficult to remove by drilling-fluid circulation. It may also aggravate bit vibration and increase the risk of cutter wear or failure. Therefore, WOB should be optimized rather than increased without limitation.

The axial acceleration under different WOB values was extracted and analyzed, as shown in Figure 20. Both the amplitude and frequency of axial acceleration increase with WOB. At WOB values of 10, 40, and 80 kN, the acceleration ranges are –0.23 to 0.22 m/s^2, –3.7 to 3.6 m/s^2, and –4.2 to 4.2 m/s^2, respectively. These results indicate that high WOB produces more severe bit vibration. Therefore, the selection of WOB should balance penetration improvement, vibration control, and cuttings-removal capacity.

Conclusion

In this study, the rock-breaking characteristics of conventional drilling and impact-scraping drilling were compared using a full-scale bit-rock finite element model. The effects of rotational speed and WOB on the rock-breaking performance of the impact-scraping drilling tool were further analyzed. The main conclusions are as follows:

1. Tensile and compressive stresses coexist in the rock under both drilling methods. Compared with conventional drilling, impact-scraping drilling produces a larger tensile-stress region and promotes stress-wave-induced rock failure. Under the baseline condition, the bit transient axial penetration velocity increases from 7.58 to 16.63 mm/s, approximately 2.2 times that of conventional drilling. Meanwhile, the average tangential cutting force decreases by 37.2%, and the tangential-force-based specific energy decreased by 38.5%, indicating that impact-scraping drilling improves both penetration performance and energy utilization.
2. Increasing rotational speed and WOB can improve the bit transient axial penetration velocity of the impact-scraping drilling tool, but their marginal benefits decrease beyond a certain range. At rotational speeds of 120, 150, and 180 rpm, the bit transient axial penetration velocity values are 16.63, 21.06, and 22.20 mm/s, respectively, while the axial acceleration amplitude increases noticeably at high speed. At WOB values of 10, 40, and 80 kN, the bit transient axial penetration velocity values increase to 16.63, 52.27, and 92.86 mm/s, respectively; however, higher WOB also intensifies bit vibration and may hinder cuttings removal. Considering penetration efficiency and vibration control, the drilling parameters should be optimized rather than increased monotonically.

Credit authorship contribution statement

Jialin Tian: Resources, Funding acquisition, Data curation, Conceptualization. Xin Li: Writing – original draft, Methodology, Investigation, Formal analysis. Chenghang Liu: Supervision, Formal analysis.

Disclosure Statement

The authors declare that they have no known competing financial interests or personal relationships that could have appeared to influence the work reported in this paper.

Declaration of funding

This work is supported by State Key Laboratory of Gas Disaster Monitoring and Emergency Technology, China (2021SKLKF07), and the Science and Technology Innovation Fund, Chengdu, China (2022-RCO3- 00005-CG).

Data availability

Data will be made available on request.

Reference

Cao W., Zhao M., Liu C., 2004. Study on the model and its modifying method for rock softening and damage based on Weibull random distribution. *Chinese Journal of Rock Mechanics and Engineering*, 23(19). DOI: 10.1007/BF02911033.

Deng Y., Guo Z., Wei Q., Wang S., 2022. Research on acceleration tool of combined impact rock breaking drilling. *Journal of Chongqing University of Science and Technology (Natural Sciences Edition)*, 24(2). DOI: 10.3969/j.issn.1673-1980.2022.02.021.

Dolezal T., Felderhoff F., Holliday A., Bruton G., 2011. Expansion of field testing and application of new hybrid drill bit. *SPE Annual Technical Conference and Exhibition*. DOI: 10.2118/146737-MS.

Dong G., Chen P., 2018. 3D numerical simulation and experiment validation of dynamic damage characteristics of anisotropic shale for percussive-rotary drilling with a full-scale PDC bit. *Energies*, 11(6), 1326. DOI: 10.3390/en11061326.

Huang H., Lu C., Ma S., Wu M., 2023. Analysis of Coupled Axial-Torsional Drill-String Vibration Based on Fuzzy Bit-Rock Interaction Model Considering Bit Balling Condition. *IEEE Transactions on Industrial Informatics*, 19(9), 9833-9842. DOI: 10.1109/tii.2022.3233664.

Huang K., Zhou C., Yang Y., Ren H., Niu Q., 2020. Working Load Characteristics of the PDC-Cone Composite Bit under Impact and Scraping. *Shock and Vibration*, 2020, 1–9. DOI: 10.1155/2020/7540519.

Ji R., Shi H., Huang Z., He W., Wu X., Fu X., Sun Z., Xiong C., 2024. A novel experimental setup for axial-torsional coupled vibration impact-assisted PDC drill bit drilling. *Review of Scientific Instruments*, 95(1). DOI: 10.1063/5.0174337.

Kong C., Wang C., Zhu R., Wang G., Liu C., Zhang D., 2022. Study on the acceleration of single cone PDC composite bit. *Mathematical Methods in the Applied Sciences*, 45(7). DOI: 10.1002/mma.8022.

Koronatov V.A., 2023. Axial–Torsional Vibrations of Drill Strings with Crush-and-Shear Hybrid Bits at Constant Tension of Suspension Cables. *Journal of Mining Science*, 59(1), 39–52. DOI: 10.1134/s1062739123010052.

Lemaitre J., 1985. A continuous mechanic model for ductile materials. *Journal of Engineering Materials and Technology*, 107(1). DOI: 10.1115/1.3225775.

Li Y., Zhang T., Tian Z., Zheng Y., Yang Z., 2021. Simulation on compound percussive drilling: Estimation based on multidimensional impact cutting with a single cutter. *Energy Reports*, 7, 3833–3843. DOI: 10.1016/j.egyr.2021.06.057.

Liu S., Ni H., Jin Y., Zhang H., Wang Y., Huang B., Hou W., 2022. Experimental study on drilling efficiency with compound axial and torsional impact load. *Journal of Petroleum Science and Engineering*, 219. DOI: 10.1016/j.petrol.2022.111060.

Liu S., Ni H., Wang Y., Zhang H., 2021. Mechanism of multi-dimensional impact loads applied in increasing the rock cutting efficiency of a PDC bit. *Journal of Vibration and Shock*, 40(2). DOI: 10.13465/j.cnki.jvs.2021.02.035.

Lu C., He Z., Chen L., Li Q., Wu M., 2023. Suppressing Coupled Axial-Torsional Vibration of Drill-String System Considering Regenerative Cutting Induced Delay and Actuator Saturation. *IEEE Transactions on Industrial Electronics*, 70(11), 11608–11617. DOI: 10.1109/tie.2022.3231288.

Mu Z., Huang Z., Sun Z., Wu X., Li G., Song X., 2022. Experimental study on dynamic characteristics of axial-torsional coupled percussive drilling. *Journal of Petroleum Science and Engineering*, 219. DOI: 10.1016/j.petrol.2022.111094.

Mu Z., Li G., Huang Z., Zang Z., 2018. Research on Axial-torsional Coupling Percussion DrillingTechnology. *China Petroleum Machinery*, 46–48(10). DOI: 10.16082/j.cnki.issn.1001-4578.2018.10.003.

Peng X., Hao S., 2021. Rock Breaking Mechanism of Composite Impact of Full-size PDC Bit Based on Finite Element Analysis. *Coal Geology & Exploration*, 49(2). DOI: 10.3969/j.issn.1001-1986.2021.02.030.

Song H., Shi H., Li G., Chen Z., Li X., 2021. Numerical simulation of the energy transfer efficiency and rock damage in axial-torsional coupled percussive drilling. *Journal of Petroleum Science and Engineering*, 196. DOI: 10.1016/j.petrol.2020.107675.

Sun Z., Huang Z., Wu X., Li G., Shi H., Mu Z., Song X., Ji R., 2024. Numerical analysis on the failure characteristics of hot dry rock subjected to axial-torsional coupled percussion with single cutter. *Geoenergy Science and Engineering*, 234. DOI: 10.1016/j.geoen.2023.212588.

Teale R., 1965. The concept of specific energy in rock drilling. *International Journal of Rock Mechanics and Mining Sciences & Geomechanics Abstracts*, 2(2). DOI: 10.1016/0148-9062(65)90016-1.

Xi Y., Wang H., Zha C., Li J., Liu G., Guo B., 2023. Numerical simulation of rock-breaking and influence laws of dynamic load parameters during axial-torsional coupled impact drilling with a single PDC cutter. *Petroleum Science*, 20(3), 1806–1827. DOI: 10.1016/j.petsci.2023.01.009.

Xi Y., Wang W., Fan L., Zha C., Li J., Liu G., 2022. Experimental and numerical investigations on rock-breaking mechanism of rotary percussion drilling with a single PDC cutter. *Journal of Petroleum Science and Engineering*, 208, 109227. DOI: 10.1016/j.petrol.2021.109227.

Yang H., Yang Y., Huang Y., Zhang H., Xie L., 2024. Development and Optimization of a High-Frequency Axial-Torsional Composite Percussion Drilling Tool for Enhanced Impact Technology. *SPE Journal*, 29(2). DOI: 10.2118/218006-PA.

Zeng Y., Liu W., Ding S., Zhu X., 2020. Numerical simulation analysis of hybrid impact cutting and its comparison with torsional impact cutting. *Journal of Vibroengineering*, 22(3), 451–464. DOI: 10.21595/jve.2019.20429.

Zha C., Liu G., Li J., Li Y., Xi Y., 2017. The Rock Breaking Mechanism of the Compound Percussive-Rotary Drilling Method with a PDC Bit. *Petroleum Drilling Techniques*, 45(2). DOI: 10.11911/syztjs.201702004.

Zhang C., Zhao Y., Gao K., Zhang C., Lv X., Xie X., 2023. Simulation and experimental investigations of ultrasonic-assisted drilling with Micro-PDC bit. *Geoenergy Science and Engineering*, 223, 211480. DOI: 10.1016/j.geoen.2023.211480.

Jialin TIAN, Ph.D.
Professor, Doctoral Supervisor
Oil and Gas Equipment Technology Sharing and Service Platform of Sichuan Province,
School of Mechatronic Engineering, Southwest Petroleum University
Chengdu, Sichuan 610500, China
E-mail: *17623162768@163.com*

Xin LI, M.Sc.
Oil and Gas Equipment Technology Sharing and Service Platform of Sichuan Province,
School of Mechatronic Engineering, Southwest Petroleum University
Chengdu, Sichuan 610500, China
E-mail: *17623162768@163.com*

Chenghang LIU, M.Sc.
Oil and Gas Equipment Technology Sharing and Service Platform of Sichuan Province,
School of Mechatronic Engineering, Southwest Petroleum University
Chengdu, Sichuan 610500, China
E-mail: *1042715288@qq.com*